ISSN 0869-5938, Stratigraphy and Geological Correlation, 2010, Vol. 18, No. 1, pp. 42–62. © Pleiades Publishing, Ltd., 2010.
Original Russian Text © A.Yu. Guzhikov, M.V. Pimenov, S.Yu. Malenkina, A.G. Manikin, S.V. Astarkin, 2010, published in Stratigrafiya. Geologicheskaya Korrelyatsiya, 2010, Vol. 18, No. 1, pp. 45–66.

Paleomagnetic, Petromagnetic, and Terrigenous–Mineralogical Studies of Upper Bathonian–Lower Callovian Sediments in the Prosek Section, Nizhni Novgorod Region

A. Yu. Guzhikov[a], M. V. Pimenov[a], S. Yu. Malenkina[b], A. G. Manikin[a], and S. V. Astarkin[a]

[a]*Geological Department, Chernyshevskii Saratov State University, Saratov, Russia*
e-mail: aguzhikov@yandex.ru
[b]*Geological Institute, Russian Academy of Sciences, Pyzhevskii per. 7, Moscow, 119017 Russia*

Received November 1, 2007; in final form April 12, 2009

Abstract—The Bathonian–Callovian boundary section located near the Prosek Settlement (Nizhni Novgorod region) is described with the characteristic of its grain-size composition and terrigenous–mineralogical, petromagnetic, and paleomagnetic properties. Based on lithological–mineralogical and petromagnetic data, the section is subdivided into four members corresponding to the most significant sedimentation rhythms. No sharp changes in the composition of sediments are noted through the section, which indicates its relative continuity. Despite the significant remagnetization of these sediments during the Quaternary, the characteristic component (ChRM) is definable by the method of the intersection of large circles. The similarity between coordinates of the calculated virtual geomagnetic pole (VGMP) and the positions of standard virtual geomagnetic poles in the stable European continent during corresponding periods serves as an important argument in favor of the primary nature of the ChRM. The compiled magnetostratigraphic section is well consistent with the paleomagnetic zonation, established in the coeval sediments of West Europe. As compared with the Bathonian–Callovian boundary section in the Albstadt–Pfeffingen of Germany, which claims to the GSSP role, the Prosek section represents a more favorable object for paleomagnetic studies. Combined with the lack of large-scale gaps in the sedimentary record and, with other conditions being equal, this makes this section a more preferable candidate for the Callovian GSSP standard.

Key words: Bathonian–Callovian boundary, magnetostratigraphy, paleomagnetism, VGMP, lithology, geochemistry, terrigenous mineralogy, grain-size composition, petromagnetism.

DOI: 10.1134/S0869593810010041

INTRODUCTION

In autumn of 2006, a group of specialists from the Saratov State University (Saratov), Geological Institute of the Russian Academy of Sciences, Ushinskii Yaroslavl State Pedagogical University (Yaroslavl), and Institute of Petroleum Geology and Geophysics (Siberian Division of the Russian Academy of Sciences, Novosibirsk) took part in the complex study of the Bathonian–Callovian boundary sediments near the Prosek Settlement (the Lyskovo administrative area of the Nizhni Novgorod region), carried out under the resolution of the Commission on the Jurassic System of the Interdepartmental Stratigraphic Committee of Russia. The purpose of this study was to obtain materials for substantiating this section as a possible candidate for a GSSP standard of the boundary between the Bathonian and Callovian stages.

The biostratigraphic data on the key fossil group (ammonites) from these sediments are discussed in (Kiselev and Rogov, 2007). In this work, we present data on their grain-size composition, terrigenous–mineralogical, petromagnetic, and paleomagnetic properties. In addition, we provide a thorough geological description of the section, which is still insufficiently characterized in the literature, since previous studies of Bathonian–Callovian boundary layers near the Prosek Settlement were largely aimed at the solution of biostratigraphic problems (Gulyaev and Kiselev, 1999; Kiselev and Rogov, 2007; and others).

To avoid possible errors and uncertainties in the interpretation of data obtained by different methods, the section was sampled for all the analyses in line with the "sample-in-sample" technique with a simultaneous geological description and paleontological study. In total, 37 stratigraphic levels were sampled in the 12.6-m-thick section. The sampling step varied from 0.2 to 0.5 m, averaging 0.3 m.

GEOLOGICAL DESCRIPTION

The Jurassic section was studied in serval ravines located along the 5-km-long slope of the Volga River valley and in the quarry near the Prosek Settlement. The section with the Bathonian–Callovian boundary is

located in the steep banr near the abandoned quarry of the brickyard (coordinates 56°06′07″N, 45°09′06″E (Fig. 1). The Jurassic sediments rest almost horizontally upon Permian strata with their boundary located at the altitude of approximately 160 m. The lower part of the section is covered by talus. Therefore, we describe below from the base upward only its upper part accessible for direct observation (Fig. 2). The description begins with bed attributed to the Upper Bathonian Cadoceras calyx Zone. Biostratigraphy and beds nomenclature are as in (Kiselev and Rogov, 2007).

Bed 1. Spotty grayish yellow sand with coloration varying from light gray to rusty and brownish, fine-grained (0.25–0.1 mm), moderately sorted, with a nest structure, oligomictic quartzose, consisting largely of subrounded quartz (less commonly feldspar and chert) grains, accompanied by single strongly altered glauconite grains and dark gray minerals, silty, clayey, micaceous, compact, with irregular thin lenticular laminae and lenses (from a millimeter to a few centimeters) of sandy to, less commonly, pure gray clays. Pure quartz sand of the same grain size, consisting of subrounded and subordinate angular grains, forms nests a few millimeters to 6 cm across in this layer. The smaller nests are characterized by capricious shapes, while the larger ones are more isometric, with some of them being round and resembling pebbles, although unlithified. Some of these nests probably represent fucoids, since there are clearly such horizontal or, rarely, vertical structures (up to 3 cm across) filled with incoherent white quartz sand. The small clay lenses crossing the bedding surfaces at oblique angles probably reflect life activity of mud-eating organisms as well. In addition, there are incoherent ferruginous inclusions up to 1 cm across and single deformed ammonite casts. In the upper part of the layer, the sediments are strongly ferruginate. The boundary with the overlying sediments is uneven, rusty in coloration, corresponding to a layer of ferruginate sand, 3 to 7 cm thick. The apparent thickness is 0.6 m.

Bed 2. The sand is gray of variable tints, beige at the weathered surface, fine-grained, moderately sorted, characterized by the more spotty texture as compared with the previous layer, oligomictic, quartzose, consisting mostly of subrounded quartz grains accompanied by dark-colored minerals, silty, clayey, micaceous, and compact, with small lenticular laminae and fragments of lenses (from a millimeter to a few centimeters), composed of gray sandy clays and areas of pure quartz sand, usually of isometric shapes (up to 15 cm across). As compared with the previous layer, the sediments are more uniform with respect to both coloration and composition. Ferrugination is manifested in the form of spots (2–4 cm in diameter) and along fissures. There are casts and impressions of ammonite and bivalve shells scattered through the layer. The sediments 30 cm below the layer top enclose two concretions: (1) small, rounded (6–7 cm in diameter), light brown, earthy at the surface and brown inside, pelitomorphic, phosphate (P_2O_5 19.6%), slightly clayey and sandy (up to 10–15% of sandy grains), and covered by a clayey–silty film; (2) large, slightly compressed (30–40 cm in diameter), carbonate, with admixture of sandy material, light, slightly ferruginate at the surface and dark gray inside, and saturated with well-preserved ammonite shells and small bivalves. The boundary with overlying sediments is similar to the previous one (ferruginate sand layer 3–5 cm thick), although more uneven. The thickness is 0.8–0.9 m.

Fig. 1. Location of the upper Bathonian–lower Callovian section near the Prosek Settlement (shown by the asterisk).

Bed 3. The sand is similar to that in Bed 1, differing from the latter in its more regular ferrugiunation and distinct bioturbation, with size- and shape-variable fucoids. In addition to small structures, there are several large (10–20 cm long) vertical and obliquely oriented fucoids filled with clay. The sediments enclose casts and impressions of ammonite and bivalve shells. The boundary with the overlying sediments represents a zone of ferruginate sand 3–5 cm thick, flatter as compared with similar zones in previous layers. Its thickness is 1.9 m.

Bed 4. The sand is similar to that in the previous layer. The lower 10 cm are less ferruginate. The sediments demonstrate intense bioturbation with the smaller (0.5–1.5 cm in diameter and up to 6 cm long) fucoids usually filled with sand in the lower part and the larger (0.8–6.0 cm across and 10–15 cm long) structures resembling *Thalassinoides* and filled with both pure white sand and clayey, frequently variegated material. Some isometric round inclusions of white quartz sand (approximately 5 cm across) are surrounded by yellow rims of jarosite (according to chemical analysis) with rare aureoles of iron hydroxides. The sediments contain casts and impressions of ammonite and rare bivalve shells. The upper boundary is ferruginate for 3–10 cm downward and is relatively uneven. Its thickness is 0.5 m.

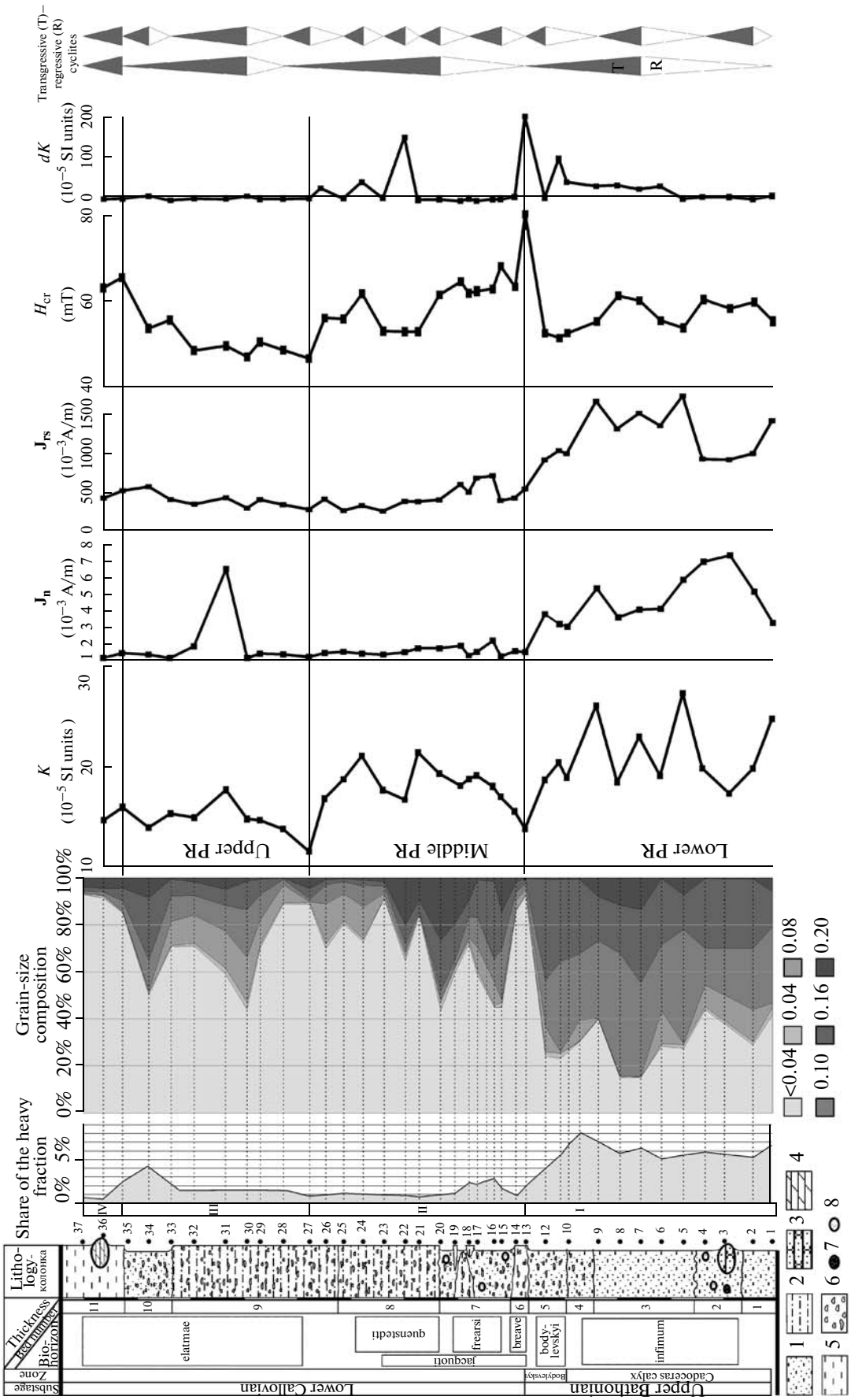

Fig. 2. The results of the grain-size, terrigenous–mineralogical, and petromagnetic studies in the Prosek section.
(I–IV) sedimentary rhythms definable based on terrigenous–mineralogical, grain-size composition, petromagnetic, and geochemical features. (PR) petromagnetic rhythms.
(1) clayey sands; (2) silts; (3) sandstones; (4) marls; (5) bioturbation; (6) phosphate concretions; (7) lenses of pure quartz sand.

Bed 5. The sand is similar to that in Bed 4, differing from the latter by its higher clay content (up to 10–25%) and lower degree of ferrugination. The lower 25 cm are almost barren of Fe oxides. The sediments are intensely bioturbated with a wide development of *Thalassinoides* fucoids and single unidentifiable crustacean remains. In addition to their generally high clay content, the sediments enclose rare lenticular layers and lenses of clayey material, whose quantity increases upward along the section. The uppermost part of the bed is composed of alternating sands and clays with the boundary of 5–10 cm being ferruginate. Ammonite casts are scattered through the entire bed. Their thickness is 0.75–0.8 m.

Bed 6. The clay is gray with a beige tint, dark gray in the wet state, and lilac-colored at the weathered surface. The lower boundary of the bed is uneven, although distinct. The clay is relatively pure, containing locally <10% sand, slightly micaceous (up to 10% of large mica flakes), vaguely bedded, and slightly conchoidal, with a shelly fracture, soaking, and plastic in the wet state. The fracture surfaces demonstrate rare microlenses (1–2-mm thick and several centimeters long) of darker clay. Some lenticular laminae (a few centimeters long) are composed of clayey sand. The sediments are notably ferruginate. The bioturbation structures are substantially different from their counterparts in the underlying beds: fucoids are narrow (2–3 mm in diameter), complex, and intricate (*Chondrites*-type), irregularly distributed, forming clots, accentuated by coloration (light gray and pale with a slight pinkish tint in the wet state). The sediments enclose small (from a few millimeters to 2 cm) limonitized concretions or their hollows with Fe hydroxides and locally yellow earthy mass (jarosite) on the walls, scattered coalified plant detritus (up to a few millimeters across), casts, and impressions of ammonite and bivalve shells. The upper boundary is uneven and slightly ferruginate. The thickness is 0.3–0.4 m.

Bed 7. The sand is irregularly colored, similar to that in Bed 5, although with a higher degree of ferrugination and a clay admixture. The lower 0.75 m are more sandy, hosting large lenses of white sand (up to 10–25-cm long and 5–10-cm thick), locally fringed by yellow material (jarosite). The clay content increases upward along the section. The middle part of the bed is composed of sand and sandy clay, alternating in the lenticular manner. Higher, there are thick (0.24–0.40 m) lenticular layers of gray (lilac-colored at the weathered surface and dark gray to chocolate in the wet state) locally variegated irregularly sandy (up to 45% sand; 20% on average) bioturbated clays with thin crusts of Fe hydroxides and rare coalified plant detritus. The sediments are intensely bioturbated with all the fucoids being flattened and the largest of them located in the lower part of the bed (0.20–0.25 m). There are also burrows and remains of crustacean organisms. The upper boundary is uneven and marked by a thin spotty–lenticular alternation of variegated sandy clays and sands, with a high to moderate clay admixture and local ferrugination. The sediments enclose numerous casts and impressions of ammonite and bivalve shells. Their thickness is 1.2–1.3 m.

Bed 8. The clay is irregularly colored gray to pale–gray, dark brown (chocolate) in the wet state, and ferruginate (spots and fissures) with spots and films of Fe hydroxides, jarosite, and Liesegang rings. The clay is irregularly sandy (5 to 25%), micaceous (up to 15%), silty (up to 15%), massive to vaguely bedded, platy, and intensely fractured, with nests (0.5–2.0 cm across) of white slightly clayey sand, small limonite concretions (a few centimeters across), and hollows (probably filled formerly with pyrite or marcasite) 10–15 cm in diameter and surrounded by ferrugination zones. The clay is characterized by high sand content (up to 40%) in the lower part of the bed, which decreases to 10–15% upward along the section to become practically pure (up to 5% of sand admixture) in its middle part. Pure varieties enclose rare microlenses up to 2-mm thick and a few centimeters long of darker clay with more distinct lamination. The clay is notably bioturbated with thin flattened tubular fucoids, probably, *Chondrites*) 1–3 to, rarely, 5 mm in diameter, filled with lighter clay or sand, locally ferruginate and fringed by jarosite (probably, formerly pyrite). There are abundant casts and impressions of ammonite and bivalve shells. Their thickness is 1.9 m.

Bed 9. The clay is gray, irregularly sandy (10 to 45% averaging 20–25%), silty (up to 15%), and micaceous (10–15%), lighter, more ferruginate, and platy as compared with that in the previous bed, locally deformed and bioturbated. The fucoids are 0.1–0.5-m in diameter and several centimeters long, filled with ferruginate, clayey, and, less commonly, pure white sand. There are coalified plant remains 0.2–0.3 mm across. The entire bed is composed of irregularly alternating lenticular laminae from a millimeter to a centimeter-thick, of variably ferruginate clays, sandy clays, and clayey sands. Similar to the previous beds, the sediments enclose microlenses of darker clays. Ammonite and single bivalve casts and impressions are scattered through the entire bed. The lower boundary of the bed is relatively distinct and even, while its upper boundary is obscure. The thickness is 3.1 m.

Bed 10. The sand is irregularly colored, largely beige with light gray (more clayey) and rusty (ferruginate) spots and lenses, fine-grained, quartzose, micaceous, silty, with variable (from 5 to 50%) clay content, irregularly bioturbated, with rare rounded nests up to 5-cm across of white quartz sand. In its characteristics, the bed resembles Bed 1. It encloses irregularly shaped lenses, nests, and lenticular laminae of sandy (20–40% of quartz grains) gray to, locally, pale clays. In the upper part of the bed, clayey spots and lenses become more abundant as compared with its other parts. There are rare impressions of ammonite and bivalve shells. The thickness is 0.9 m.

Bed 11. The clay is gray with a beige tint, dark gray with chocolate tint in the wet state, with pale spots at the weathered surface, relatively pure (locally with 5–10% of sand), slightly silty (up to 5%) and micaceous (up to 5% of large flakes), massive to, locally, obscurely bedded, platy, intensely fractured, soaking, and plastic in the wet state. In some layers, the clay contains a higher (up to 20–25%) admixture of sand and rare thin (0.5–1.5 cm) lenses of light clayey sand. The bed encloses ichnofossils in form of branching tubes 1.5–3.0 mm in diameter, with ferrugunate edges, usually hollow (probably, *Chondrites*). Approximately 0.4 m above the bed base, there is a rounded almost spherical dark gray carbonate concretion 20–25 cm across with rare small bivalve shells and small (<1mm) rounded inclusions of fine-grained pyrite with their maximal concentration in the central part, where the rock is bleached. The bed contains occasional impressions of ammonite and bivalve shells. The apparent thickness is 1.1 m.

As follows from this description, the main component of the section is represented by *terrigenous* sandy and clayey (with variable silt admixture) sediments, with rare authigenic usually altered sulfides and single phosphate structures. The sandy and silty fractions are compositionally uniform, being represented by dominant quartz, subordinate mica, accessory feldspars, and single intensely altered glauconite grains. The lower five beds of Bathonian age are entirely composed of irregularly clayey sands. The overlying Callovian sequence begins with pure clays and is largely characterized by a clayey composition.

For determining the **mineral clay composition**, we studied a collection of samples taken from all the clayey layers of the section in the Laboratory of Physical Analytical Methods (GIN RAS) by the X-ray diffraction method. It was established that the main minerals (in decreasing order) are kaolinite, micaceous mineral (with single swelling layers), defective chlorite, smectite, gypsum and, probably, metahalloysite (the last two minerals occur in trace quantities). Some samples also demonstrate an admixture of quartz and feldspars.

Sulfide concretions (pyrite or marcasite) are usually replaced by iron hydroxides and oxides (limonite), gypsum, and jarosite. The same is true of pyritized fucoids and faunal casts. The intense ferrugination of layers, limonitization, and jarositization of concretions, faunal remains, and ichnofosils are largely determined by supergene oxidation of Fe sulfides, which implies a wide development of reducing conditions in sediments during diagenesis. This assumption is consistent with the occurrence of *Chondrites*, which indicate calm sedimentation settings and lowered oxygen concentrations in sediments (Seilacher, 2007). Limonitized hollow concretions with a jarosite infill, occurring within clays as well as small isometric rounded lenses in some sand layers are surrounded by bright yellow rims of jarosite or yellow rims with aureoles of Fe hydroxides and, less commonly, limonite crusts, which probably reflect the complete decomposition and replacement of sulfide concretions.

The content of **organic matter** in both Bathonian and Callovian sediments is negligible. According to the chemical analysis performed at the Laboratory of Chemical–Analytical Studies (GIN RAS), the C_{org} concentrations in them are usually below 0.6%. The content of **carbonate material** in both sandy and clayey varieties is also insignificant.

The distribution of chemical elements in the beds demonstrates significant variations in their concentrations. Some of them (Fe_2O_3, MgO, K_2O, and, in most layers, MnO, Ti, Zn, Cu, Ni, Co, V) are distinctly correlative with Al_2O_3 concentrations, which indicates their relation with alumosilicates. Minor elements such as Sc, Nb, Th, Y, and Rb also demonstrate a distinct tendency for sorption by clays with the Sc content in clay layers exceeding the background one. The elevated Ba concentrations are usually considered as reflecting high bioproductivity. In the sediments under consideration, its contents are twice as low as compared with clarke concentrations and are distinctly correlative with Al_2O_3, which indicates its transportation from land sources together with clays. Na_2O and Zr entered oligomictic quartz sands mainly together with feldspars and zircons, respectively. Other elements are strongly correlated with the SiO_2 and sand layers. A notable positive correlation with SiO_2 is characteristic of Pb, Sr, and F, while S and usually Ca demonstrate negative correlations. Arsenic is partly correlative with S. As a whole, the distribution of most elements is determined by the intensity of the terrigenous transportation into the basin, the proximity of the shore and, thus, an alternative supply of fine-grained or coarse-detrital alumosiliciclastic material; i.e., by sea level fluctuations. The sharpest changes are registered at sampling levels 13, 14, 34, and 35; and less notable changes are observed approximately between sampling levels 26 and 27.

GRAIN-SIZE AND MINERALOGICAL STUDIES

Figure 2 presents **the results of the grain-size analysis** conducted by the sieve method. The most significant changes in the plots demonstrating the distribution of the grain-size composition through the section are connected with the dominant fraction <0.04 mm (up to >90%) and minimal contents of larger mineral particles. They are observable at levels of samples 13, 14 (Bed 6, the base of which corresponds to the Bathonian–Callovian boundary), 27, 28 (the basal part of Bed 9, the base of the *elamatae* biohorizon) and 35–37 (the base of Bed 11, the *elamatae* biohorizon).

The Bathonian part of the section (beds 1–5) is characterized by the minimal content of particles <0.04 mm in size (approximately 20–40%). The Callovian interval (beds 6–11) is usually dominated by the

pelitic fraction (particles <0.04-mm across constitute 50–90% of the rock volume). Thus, the main features in the distribution of the composition of the grain-size indicate the regressive stage in the development of the late Bathonian basin (the high contents of inequigranular psammitic material in beds 1–5) and transgressive development of the basin during the early Callovoian (the prevalence of pelitic material in beds 6–11). These inferences are consistent with traditional concepts of Russian Plate paleogeography (Sazonova and Sazonov, 1967), according to which the Callovian transgression was triggered by tectonic subsidence of the crust and was controlled by the fluctuation of the eustatic sea level (Sahagian et al., 1996; Sandoval et al., 2001). Sea-level changes in the Middle Volga region were most likely governed at the Bathonian–Callovian transition by both tectonic and eustatic factors.

The Callovian part of the section demonstrates additional rhythmical changes in the grain-size composition, determined by variations in the share of the pelitic fraction: a decrease in intervals corresponding to samples 15–22 and 29–34 and an increase at levels of samples 21–28 and 35–37. The analysis of available materials on concentrations of clay minerals and grain-size (Fig. 2) composition reveals several cyclites. The complete cycle includes a pair of cyclites: regressive and transgressive, whose alternation is subordinate to the rhythms determined by intermittent shoaling and deepening of the basin (Karagodin, 1980). Three large sedimentary cycles complicated by smaller varieties are outlined in the section with their boundaries corresponding to sampling levels 13, 27–28, and 35. The relative increase in the smectite content in samples 13, 28, and 32 reflects local peaks of the transgression, i.e., maximal sea-level rises. The development trend of the basin during the period corresponding to the interval under consideration shows that the first stage was marked by extremely shallow settings with high-energy hydrodynamics, which is evident from the occurrence of *Thalassinoides* (Seilacher, 2007) and the prevalence of sandy fractions. Due to the initiated transgression at the end of this stage near the Bathonian–Callovian transition, the *Thalassinoides* were replaced by the *Chondrites*, which are indicative of calm sedimentation settings with a lowered oxygen content in bottom waters (Seilacher, 2007). At the second stage, the transgression was intermittently interrupted by local regressions, although its tendency continued. The third stage was generally characterized by the transgressive trend, despite the fluctuation in the local sea level. The fourth stage was marked by the wide development of transgression. All these events are strongly consistent with other data on sea-level fluctuations on the Russian Plate in the period under consideration (Sahagian et al., 1996).

The **mineral composition of the heavy fraction** was analyzed in 17 samples taken from different levels of the section. It is established that regardless of the composition of the grain-size, the highest share of heavy fraction is provided by the fraction 0.04–0.08 and 0.08–0.1 mm. The heavy fraction is represented by both stable and unstable minerals, with the latter being dominant. According to Table 1, the distribution of minerals through the section demonstrates certain regularities. Zircon, rutile, tourmaline, kyanite, anatase, ilmente, leucoxene, and epidote occur practically in all the examined samples. The different behavior is characteristic of garnet, staurolite, sphene, amphiboles, and pyroxenes: they occur in 50% of the samples, where their content is <0.5%.

The analysis of proportions between minerals of the heavy fraction (Tables 1, 2) and its percentage (Fig. 2) allows four members to be defined in the examined section, with boundaries corresponding to the levels of the most distinct changes in the rain-size composition of the rocks (Fig. 2).

In Member I (samples 1–12), the share of zircon, rutile, leucoxene, and ilmenite is 35–40, 7–10, 1.5–3.5, and 12–13%, respectively. Garnet (0.01–0.5%) occurs only in this member; the limonite content is <1%, epidote averages 31%, and amphiboles and pyroxenes constitute 0.01–0.5%. The share of the heavy faction in this member is maximal and amounts to 8%.

Member II (samples 13–26) is characterized by the low contents of stable minerals. For example, the zircon content rapidly decreases to 4% to become 3% in Sample 17. The rutile concentrations also decrease to 0.4%, although in the last sample, it increases again up to the maximal values for the entire section (35%). Kyanite demonstrates a decrease in its contents of up to 0.02%, except for Sample 17, where its concentration reaches maximal values (4.1%). As a whole, the member is characterized by the increased share of ilmenite of up to 23% and even to 31% in Sample 17. The epidote distribution differs from that in the previous member, increasing to 44%. The member demonstrates an increased role of slightly stable and unstable minerals, except for Sample 17, where the role of stable minerals increases, while the unstable minerals are practically missing. The share of the heavy fraction in this member is low, ranging from 3% in its lower part to <1% in the top layers.

In its main mineral distribution patterns in the heavy fraction, Member III (samples 27–35) is similar to Member I, except only for the occurrence of staurolite (up to 0.12%), an increased share of leucoxene (up to 4%), anatase (up to 0.6%) and kyanite (up to 3%), and a decreased content of epidote (up to 20%). The content of the heavy fraction slightly increases as compared with the previous member (up to 1.5%), reaching maximal values in the uppermost part of Member III (up to 4%).

In Member IV (samples 36, 37), the share of rutile, tourmaline, kyanite, and ilmenite decreases, while the concentration of epidote increases; the share of the heavy fraction is minimal (approximately 0.5%).

Table 1. Contents (%) of minerals in the heavy fraction from the upper Bathonian–lower Callovian sediments of the Prosek section

Sample number	Stable minerals												Unstable minerals			
	Zr	Rut	Tour	Di	Ants	Lc	Ilm	Gr	St	Lim	Sph	Hem	Ep	Amph	Px	Bi, Musc
37	38.5	4.01	0.06	0.01	–	4	10.5	–	–	0.06			35	–	–	0.01
35	35	11.5	1.5	2.0	0.01	3.5	15.5	0.06	0.01	0.06	0.01	0.12	20	0.01	0.06	0.01
34	38	13.5	1.0	3.0	0.06	4	14.0	–	–	0.06	–	–	28.5	0.01	0.01	0.12
31	36	12.5	1.5	3.0	0.5	4	16	–	–	0.06	–	–	28.0	0.01	0.01	0.12
29	37	13	1.5	2.5	0.6	2	16.5	–	0.12	0.06	–	–	27.0	0.01	0.06	0.01
27	33.5	12	1.5	2.5	0.5	2	18.5	–	0.12	0.06	–	–	26.5	0.01	0.06	0.01
21	4.06	1.06	1.0	0.02	–	0.06	23.0	–	-	19	–	0.01	44.06	–	0.01	0.02
19	5	0.4	1.5	0.05	0.01	0.06	13.0	–	0.12	39.0	0.12	–	43.0	–	–	0.07
17	3	35	1.0	4.06	0.01	10	31.0	–	–	0.06	–	0.12	–	0.01	0.01	–
14	6	0.3	1	0.06	0.01	0.05	12.0	–	0.12	39.0	0.12	–	38	–	–	0.06
13	6.06	0.27	1	0.06	0.01	0.05	12.0	–	0.12	39.0	0.12	–	36	–	–	0.07
10	35	7.0	1.5	1.0	0.2	1.5	15.0	0.5	–	0.06	–	0.06	33.0	0.5	0.5	0.18
8	35.5	6.56	1.5	1.0	0.2	1.5	15.5	0.5	–	0.06	–	0.06	33.0	0.5	0.5	0.18
7	36.5	10.05	0.5	1.5	0.06	3.5	11.5	0.01	–	0.06	–	0.12	32.0	0.01	0.01	0.13
5	37	9.5	1.0	0.01	0.03	3.5	12.0	0.01	–	1.0	–	0.06	31.0	0.01	0.01	0.13
4	39.5	8.06	1.5	0.01	0.01	3.0	12.0	0.01	–	1.0	–	0.06	30.06	0.01	0.01	0.01
2	38	8	1.0	0.01	0.01	3.0	11.5	0.01	–	1.0	–	0.05	30.05	0.01	0.01	0.01

Note: Mineral symbols: (Zr) zircon, (Rut) rutile, (Tour) tourmaline, (Di) kyanite, (Ants) anatase, (Lc) leucoxene, (Ilm) ilmenite, (Gr) garnet, (St) staurolite, (Lim) limonite, (Sph) sphene, (Hem) hematite, (Ep) epidote, (Amph) amphiboles, (Px) pyroxenes, (Bi) biotite, (Musc) muscovite). For sampling levels, see Fig. 2.

Table 2. Mineralogical and petromagnetic characteristics of the Prosek section

Interval	Su.m./Ss.m. coefficient		K, 10^{-5} SI units	$\mathbf{J_n}$, 10^{-3} A/m	$\mathbf{J_{rs}}$, 10^{-3} A/m	H_{cr}, mT	dK, 10^{-5} SI units
	Average values	Variations					
IV (Sample 36–37)	0.6	0.59–0.63					
III (Sample 27–35)	0.4	0.4–0.39	11.86–17.68 / 14.82	1.01–6.46 / 1.81	279–652 / 414	47.1–66.08 / 52.21	–10.3…–2.29 / –6.24
II (Sample 13–26)	0.8	0.71–0.92	113.8–21.73 / 18.11	1.12–2.08 / 1.44	270–739 / 470.5	53.45–80.79 / 61.74	–11.46…+199.5 / 21.62
I (Sample 2–12)	0.5	0.48–0.64	16.94–26.97 / 20.77	2.93–7.3 / 4.69	918–1753 / 1239.9	51.88–61.77 / 56.94	–12.6…+94.02 / 18.34

Note: (Su.m.) sum of unstable minerals; (Ss.m) sum of stable minerals; numerator designates minimal and maximal values, denominator shows average values of petromagnetic parameters.

The coefficient of stability, calculated as the ratio between the sum of the unstable and the sum of the stable minerals, varies through the section (Table 2), repeating the regularities, derived from the analysis of the grain-size, mineral compositions, and the distribution of the heavy fraction (Fig. 2).

Thus, the terrigenous-mineralogical analysis reveals no qualitative changes in the composition of minerals in the heavy fraction, which implies a single main source of terrigenous material at the Bathonian–Callovian transition. It is conceivable that northern land represented such a source, since the mineral spectrum in the heavy fraction of the examined samples is very similar to that in the crystalline rocks of the Baltic Shield, where the heavy fraction is dominated (>50%) by epidote, kyanite, staurolite, zircon, tourmaline, and rutile. The inference of the decisive role of the Baltic Shield in the supply of terrigenous material

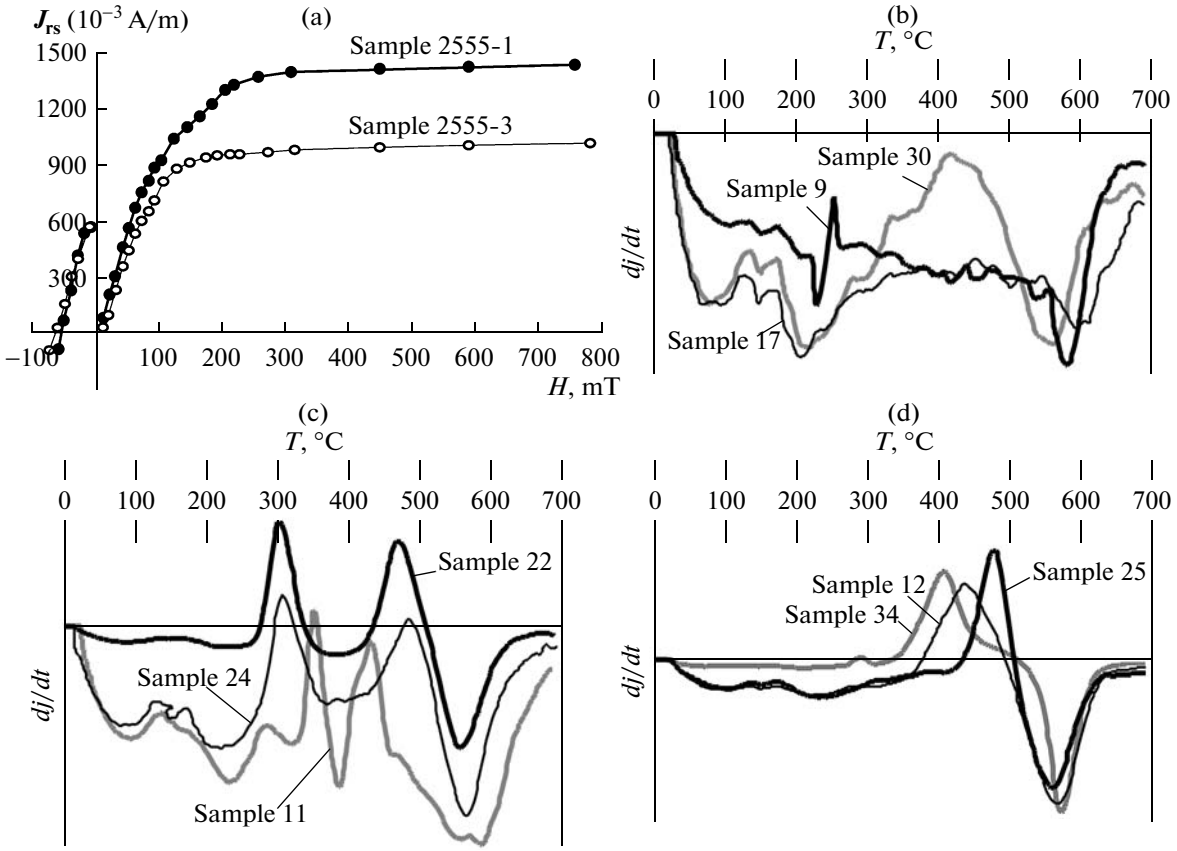

Fig. 3. Results of the magnetic–mineralogical analysis: curves (a) of magnetic saturation and (b–d) differential TMA (first derivatives from TMA curves).

into the Late Bathonian and early Callovian basins in the Prosek section area is consistent with available paleogeographic reconstructions (Grossgeim, 1972; Grossgeim et al., 1984), where the Middle Volga region is considered as an element of the Moscow terrigenous–mineralogical province. It should be noted that, according to the data of these authors, the Callovian Age was marked by the intensified transportation of terrigenous material from the Urals, although information derived from the Prosek section is insufficient for either the substantiation or rejection of this inference.

PETROMAGNETIC AND MAGNETIC–MINERALOGICAL STUDIES

The petromagnetic and magnetic–mineralogical studies were aimed at assessing rock samples for paleomagnetic measurements and obtaining additional information on the distribution of the ferromagnetic fraction and finely dispersed iron sulfides, which was used, along with geochemical and lithological–mineralogical criteria, for revealing and substantiating the sedimentary rhythmicity in the section. These studies performed at the Laboratory of Petrophysics of the Saratov State University included measurements of magnetic susceptibility (K), its anisotropy, and natural remanent magnetization ($\mathbf{J_n}$), experiments with magnetic saturation with subsequent determination of the remanent saturation magnetization ($\mathbf{J_{rs}}$) and remanent coercive force (H_{cr}), thermal kappametry, and thermomagnetic analysis (TMA). The magnetic susceptibility and remanent magnetization were measured at the device MFK-1B (kappa bridge) and spinmagnetometer JR-6, respectively; the thermal analyzer TAF-2 ("magnetic weights") was used for the thermomagnetic analysis.

The magnetic hard phase connected with iron hydroxides is reflected in the insignificant, although progressive growth of $\mathbf{J_{rs}}$ in high-intensity fields (up to 700 mT) (Fig. 3a), elevated H_{cr} values (>80 mT) (Fig. 2), and characteristic declines in magnetization under temperatures of 100–200°C, which are distinctly seen in differential TMA curves (Fig. 3b). Supergene genesis of $Fe(OOH) \cdot nH_2O$ is evident from the decreasing intensity of rock ferrugination away from the surface. Unfortunately, we failed to sample "pure" (lacking visible signs of chemical weathering) rocks despite the relatively deep (up to 1 m) pits.

Magnetite and relative minerals are reliably identified in differential TMA curves, owing to the sharp

Table 3. Coefficients of linear correlation between values of petromagnetic parameters and percentages of different grain-size particles

Grain size, mm	Petromagnetic parameters			
	K	$\mathbf{J_n}$	$\mathbf{J_{rs}}$	H_{cr}
<0.04	*−0.54*	*−0.61*	*−0.76*	0.05
0.04	0.10	−0.01	−0.12	−0.13
0.08	−0.10	−0.12	−0.22	−0.31
0.10	**0.60**	**0.61**	**0.87**	−0.11
0.16	0.38	**0.52**	**0.62**	0.01
0.20	0.19	−0.05	0.09	0.15

Note: The examined selection includes 36 samples (N). Significant correlation coefficients at the significance level (p) 0.01, indicating positive and negative correlations are shown in bold and italic, respectively.

declines in magnetization close to the Curie point of Fe_3O_4 (578°C) (Fig. 3b) as well as the relatively low values of the saturation fields (80–250 mT) and of the coercive force (40–50 mT), which indicate the magnetically soft phase (Fig. 2). In addition, some samples of sandy–silty varieties contain magnetite grains (approximately 0.1 mm across), which is established under the binoculars; the degree of their roundness unambiguously indicates the terrigenous origin of Fe_3O_4.

The increase in the magnetic susceptibility after sample heating (dK) is related to the admixture of Fe sulfides or carbonates, which are transformed into highly magnetic magnetite at 500°C. The TMA curves demonstrate admixture of pyrrhotite at three levels of the section (samples 11, 22, and 24), which is identified owing to increased magnetization at 300–350°C (Fig. 3c). The occurrence of pyrite is reflected in increased magnetization at temperatures exceeding 380–450°C in many samples (Fig. 3d), although an increase in magnetic susceptibility (from 18 to 200×10^{-5} SI units) is not universal. High dK values are registered in samples with maximal Fe sulfide admixtures. Other samples demonstrate an insignificant decrease, rather than an increase of magnetic susceptibility (up to 10×10^{-5} SI units), which is explained by the oxidation of the magnetic grains. The lack of increase of K, despite the admixture of pyrite (according to TMA data), indicates an extremely low content of its presumably fine-grained fraction: the increase in magnetic susceptibility on account of newly formed magnetite cannot compensate, due to extremely low FeS_2 concentrations in such samples, the decrease in K owing to the martinization of the primary Fe_3O_4 grains, which is unavoidable under long heating. The fine-grained pyrite fraction may be identified by the thermal magnetic analysis, when sample heating lasts several minutes. At the same time, the resulting magnetite may be oxidized during an hour-long heating, particularly in incoherent sediments. The finely dispersed state of pyrite and pyrrhotite particles is indirectly confirmed by the fact that their occurrence is not registered by the examination of the heavy fraction under binoculars. As was mentioned, a significant share of the iron sulfides was most likely destroyed by supergene processes.

The sediments under consideration are characterized by low K ($12–27 \times 10^{-5}$ SI units) and $\mathbf{J_n}$ ($1–7.3 \times 10^{-3}$ A/m) values (Fig. 2, Table 2). By its magnetic susceptibility, the section is divisible into three rhythms, with boundaries marked by local minimums of this parameter and strongly consistent with the most significant changes in the H_{cr} plot (Fig. 2, Table 2). The $\mathbf{J_{rs}}$ plot (Fig. 2) demonstrates a distinct trend of decreasing magnetization of the remanent saturation upward along the section. A similar tendency, although with a sharper change in its values at the boundary between beds 5 and 6, is also observable in the $\mathbf{J_n}$ plot (Fig. 2, Table 2). The magnetic susceptibility depends on the concentration of both ferromagnetic and paramagnetic materials in the rocks. Moreover, under K values of $< 20 \times 10^{-5}$ SI units, the contribution of the paramagnetc fraction (most minerals belong to the latter) may be decisive. The values of the remaining parameters are determined only by ferromagnetics. The remanent coercive force depends on both the development of the hard magnetic phase (iron hydroxides) and the grain-size composition of the magnetic particles. It is conceivable that the elevated H_{cr} values (Fig. 2), characteristic of the average petromagnetic rhythm, are explained by the minimal grain size of the Fe_3O_4 particles in this interval.

A comparison between the petromagnetic data and the rain-size composition shows that the distributions of $\mathbf{J_{rs}}$ and $\mathbf{J_n}$ (whose variations in the sediments under consideration are determined by magnetite) are correlated to the content of the fraction 0.1–0.16 mm (Table 3). This fact allows one to make the unambiguous inference that the main share of the magnetic soft faction is confined precisely to this fraction. Such a correlation does not mean that all the Fe_3O_4 particles are 0.10–0.16-mm across. On the contrary, large magnetite grains approximately 0.1-mm across and with a degree of roundness, unambiguously indicating their terrigenous origin, are recorded under binoculars. The main share of ferromagnetics occurs in the form of inclusions in terrigenous particles 0.10–0.16-mm in size. Their almost complete absence in the finely dispersed faction is reliably confirmed by the significant negative correlation of the $\mathbf{J_{rs}}$ and $\mathbf{J_n}$ values, with the content of particles <0.04-mm across (Table 3). Variations in the plot of the remanent saturation magnetization most distinctly reflect changes in the concentrations of the magnetite grains and, consequently, of particles 0.10–0.16 mm in size through the section (since the $\mathbf{J_n}$ values are influenced by the orientation of the magnetization vectors, in addition to the concentrations of ferromagnetics), which make it possible to

reconstruct fluctuations in the intensity of the terrigenous transportation into the paleobasin.

Based on all the petromagnetic parameters, the section is divisible into three rhythms (lower, middle, and upper), which practically coincide with members I–III, defined by using terrigenous–mineralogical and grain-size composition criteria (Fig. 2, Table 2). In the upper part of the section, determinations of magnetic properties were obtained only for a single level (Sample 36); therefore, the petromagnettic rhythm corresponding to Member IV is unidentifiable.

Thus, petromagnetic data provide, along with other lithological features of rocks, additional substantiation of sedimentary rhythms in the section and their individualization.

PALEOMAGNETIC STUDIES

The paleomagnetic studies were aimed at revealing the variation of the magnetic polarity through the section and included measurements of natural remanent magnetization of samples after several successive magnetic cleanings by the variable field (up to 80–100 mT with a step of 5 mT), which were performed on the device 2G Enterprises in the Institute of Geology of the Czech Academy of Sciences (Prague). The component analysis of the obtained data was conducted in the Laboratory of Petrophysics of the Saratov State University, using the program Remasoft 3.0.

The selected collection of samples represents an extremely complex paleomagnetic object. On the one hand, the study of anisotropy in magnetic susceptibility revealed the magnetic structure, typical of sediments that accumulated in hydrodynamically calm settings (the short axes of the magnetic ellipsoids are concentrated in the center of the stereoprojection, while the long axes are regularly oriented along the equator) (Fig. 4), which represents a favorable prerequisite for obtaining paleomagnetic information. On the other hand, the occurrence of a significant admixture of supergene iron oxides in sediments, in addition to magnetite, indicates the high probability of the remagnetization of the rock.

The magnetic cleanings and measurements of remanent magnetization were conducted with a high quality, which is evident from the demagnetization curves (persistent decrease in the $\mathbf{J_n}$ values in parallel with the growth of the intensity field), observed in the stereoprojections and Zijderveld diagrams, where the rectilinear segments of the lines, approximating successions of points, are characterized by maximal deviation angles (MDA) of 15°, being usually <10° (Fig. 5). The Zijderveld diagrams demonstrate largely the two-component (less commonly, three-component) composition of natural remanent magnetization. The low-coercivity component (LCC) is mostly destroyed in fields <15–25 mT, while the high-coercivity component (HCC) is definable mainly in fields 20–30 mT and preserved in fields up to 80–100 mT. In some samples, the intermediate component is definable, for example, in Sample 5 (Fig. 5) in the fields ranging between 25 and 40 mT, with direction D = 81.7°, the parameters I = 52.5°, MDA = 7.8°, LCC (D = 210.7°, I = 71.6°, MDA = 7.8°), and HCC (D = 220.9°, I = 20.1°, MDA = 10.3°) are located, together with all the $\mathbf{J_n}$ directions on the arc of the large circle, which indicates the significant contribution of the intermediate component to sum of the magnetization of this sample. The stereoprojections provide an impression that the third component in some samples is definable after the impact of strong fields (>50 mT) and corresponds to the direction close to that of the present-day magnetic field or one of the other characteristic remagnetization directions (for example, in samples 3, 23, 25, and 31) (Fig. 5). The analysis of Zijderveld diagrams prevents, however, the reliable identification of this component (the MDA exceeds 20°–30°). The strong scatter of the $\mathbf{J_n}$ vectors in high fields may be explained by the extremely low values of remanent magnetization; in any case, judging from the Zijderveld diagrams, these HCC values do not contribute much to the sum of the natural remanent magnetization and they can be omitted from the component analysis.

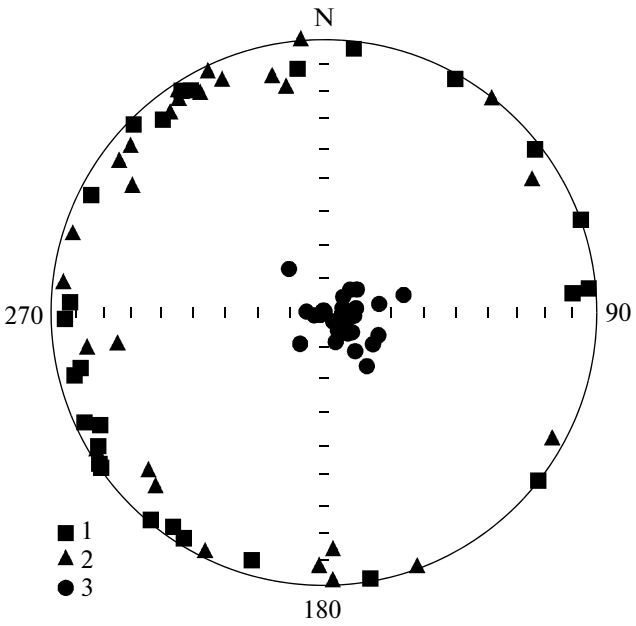

Fig. 4. The distribution of directions of axes determined for ellipsoids of the magnetic susceptibility anisotropy in the geographic coordinate system: (1) maximal, (2) intermediate, (3) minimal.

As expected, it appeared impossible to completely destroy the hard component, related to iron hydroxides, even by variable magnetic fields up to 140 mT. Practically in all the Zijderveld diagrams, the rectilinear segments, corresponding to the high-coercivity component do not converge in the center of the coordinates, which implies the incomplete destruction of one or several components. It seems that only the con-

Fig. 5. Results of the component analysis for the Prosek section (from the left to right): stereographic illustrations of changes in $\mathbf{J_n}$ vectors during cleaning by the variable magnetic field, Zijderveld diagrams (in the geographic coordinate system), plots of sample demagnetization.

Projections of $\mathbf{J_n}$ directions: (1) on the lower hemisphere; (2) on the upper hemisphere.

ditionally named LCC component is partly destroyed in the low fields, while its other part is preserved in the high fields and, thus, distorts the direction of the high-coercivity component. In their purest form, the high-coercivity components are definable in clay samples (for example, samples 23 and 25) and in Sample 3 taken from the sandstone concretion cemented by clayey–carbonate cement (Fig. 5).

The different degrees of contamination of the high-coercivity component of $\mathbf{J_n}$, connected with hard ferromagnetic, is evident from the distinct confinement of many HCC vectors in the resulting stereogram to planes of large circles (LC) (Fig. 6a). In addition, the $\mathbf{J_n}$ directions in many samples migrate regularly along arcs of large circles during magnetic cleanings (Fig. 5).

It may be expected that rock remagnetization, determined by supergene changes could have occurred in the recent geological epoch, although the HCC vectors are largely inconsistent with the direction of the recent geomagnetic field, varying within wide limits (Fig. 6b).

We believe that the rocks were remagnetized during one of the geomagnetic excursions, probably, Gothenburg, which happened at the Neopleistocene and Holocene transition ~12 ka ago and coincided with the termination of the last glaciation epoch of the Quaternary Period (*Additions* ..., 2000; Pospelova, 2000). The climatic warming was accompanied by maximal moistening of the sediments in the uppermost part of the crust section, related to both the thawing of permafrost and the appearance of large quantities of infiltration waters. The intense oxidation of rocks in different rock layers was characterized by different intensities, for example, due to more rapid thawing of surface layers, as compared with the subsurface strata and faster saturation of pure sands by infiltration waters, as compared with clayey sediments. During the transformation of the upper Bathonian and Callovian strata by oxidation processes, the geometry of the geomagnetic field could change several times, owing to the rapid migration of the pole during the excursions and different layers could preserve different magnetization vectors, determined by iron hydroxides (Fig. 6c).

The proposed model of the formation of the LCC, which is internally consistent, is supported by similar distribution patterns of its vectors on the projection sphere (Fig. 6b) and directions of the geomagnetic field in the Middle Volga region, which correspond to different positions of the magnetic poles during the Gothenburg epoch (Fig. 6d). When calculating directions, we used the geographic coordinates of the Prosek section and the coordinates of the magnetic poles for the Gothenburg excursion in (Tretyak, 1983).

Substantial differences in the remagnetization directions in different layers and regular migrations of the $\mathbf{J_n}$ directions along arcs of large circles in many samples during magnetic cleaning (Fig. 5) provide favorable prerequisites for applying the method of the intersection of large circles (Halls, 1076) for a more accurate determination of the directions for the stable (characteristic) ChRM component of $\mathbf{J_n}$. The use of this method is based on the assumption that vectors of primary magnetization are characterized by the higher interlayer parameter of accuracy, as compared with the remagnetization vectors. Taking into consideration, the significant scatter of the LCC vectors (Fig. 6b), this assumption seems highly probable.

When approximating trajectories of changes in the $\mathbf{J_n}$ directions during magnetic cleanings by the LC arc, we used at least four points (usually 7–10 points). No large circle was determined, if an angle between LCC and HCC vectors was <25° (for example, Sample 25 in Fig. 5).

The intersection of all the calculated circles yields the direction, close to that of the HCC vectors in samples 3, 23, and 25, for which the most reliable Zijderveld diagrams are obtained (Fig. 7, Table 4). The rejection of large circles, based on different criteria (i.e., exclusion from the analysis of large circles, which correspond to sands or are characterized by the MDA value exceeding 15°), result in no substantial changes of the ChRM direction, derived from the intersection of the large circles (Fig. 7, Table 4). The coordinates of the calculated virtual geomagnetic poles, based on the ChRM vectors, determined in such a manner are close to the positions of the standard virtual geomagnetic pole during the Middle Jurassic (all of them fall into confidence circles of standard poles (Fig. 8, Table 4)).

The most accurate ChRM direction was likely obtained by the LC intersection with MDA < 15°, which is characteristic only of clayey samples (Table 4). The pole position based on this direction practically coincides with the coordinates of the standard virtual geomagnetic poles of stable Europe, available for the period of 165–170 Ma ago (Besse and Courtillot, 2002), which represent a strong argument in favor of the primary nature of the defined magnetization component.

At the same time, the substantiation of the ChRM's primary nature does not solve the problem of the old field's polarity, since the large circles intersect each other at two points, differing by 180° (Fig. 7, Table 4). For determining the polarity as representing the main criterion, we used the angle distance (Δ)

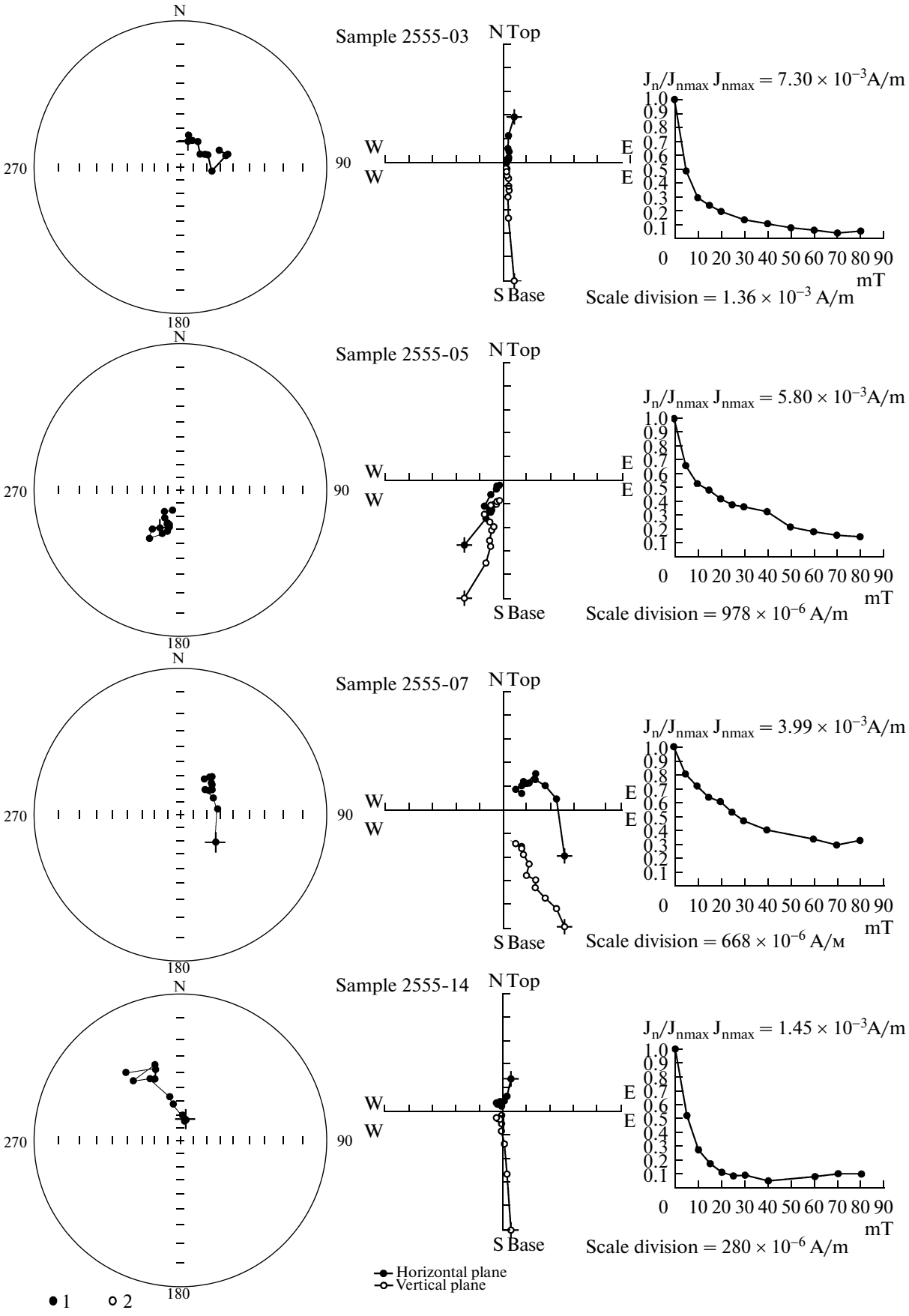
N
270
90
180
Sample 2555-03
N Top
W
W
E
E
S Base
J_n/J_{nmax} $J_{nmax} = 7.30 \times 10^{-3}$A/m
1.0
0.9
0.8
0.7
0.6
0.5
0.4
0.3
0.2
0.1
0 10 20 30 40 50 60 70 80 90
mT
Scale division = 1.36×10^{-3} A/m
Sample 2555-05
N Top
S Base
J_n/J_{nmax} $J_{nmax} = 5.80 \times 10^{-3}$A/m
Scale division = 978×10^{-6} A/m
Sample 2555-07
N Top
S Base
J_n/J_{nmax} $J_{nmax} = 3.99 \times 10^{-3}$A/m
Scale division = 668×10^{-6} A/м
Sample 2555-14
N Top
S Base
J_n/J_{nmax} $J_{nmax} = 1.45 \times 10^{-3}$A/m
Scale division = 280×10^{-6} A/m
Horizontal plane
Vertical plane
1
2

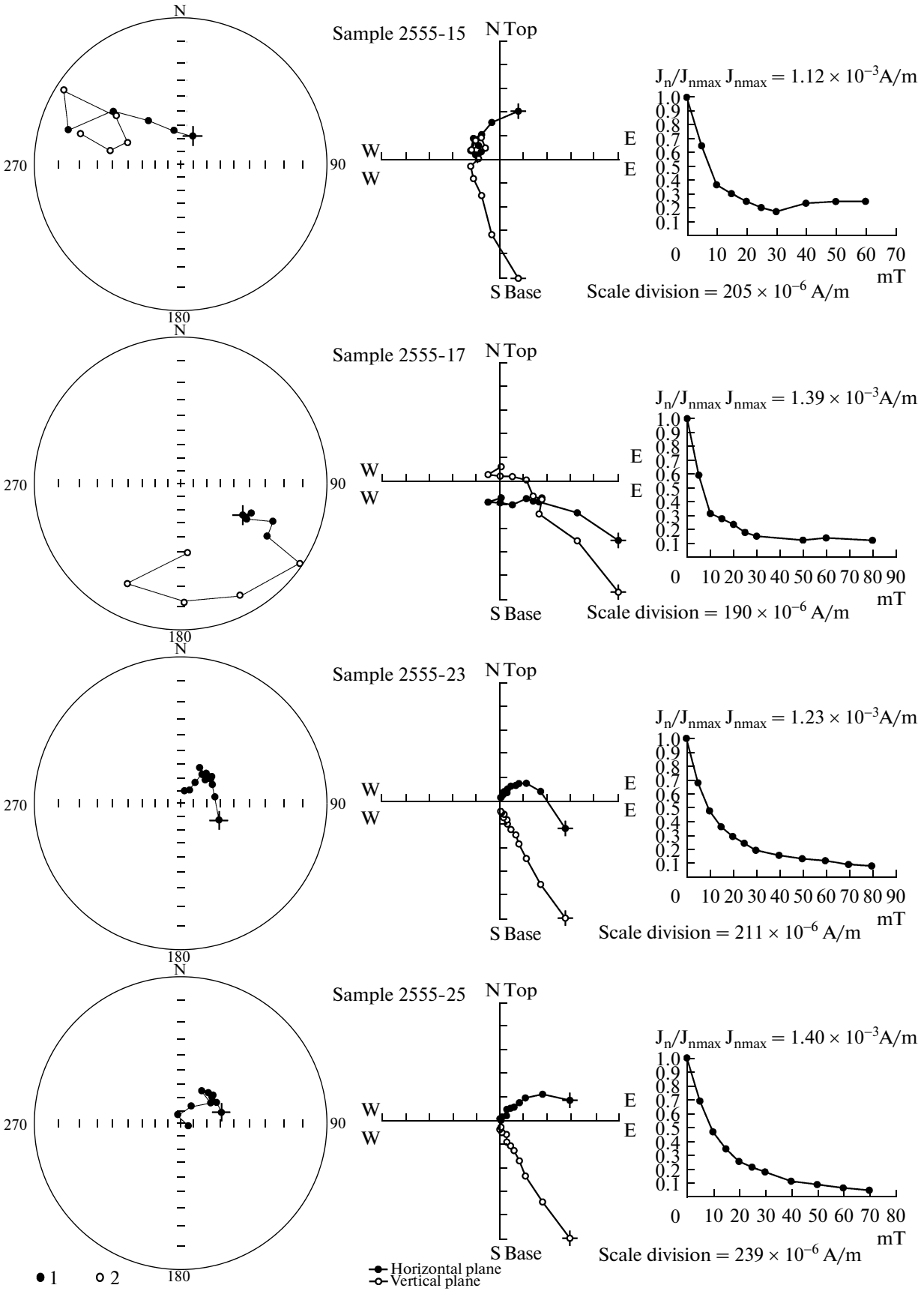
N
270
90
180
Sample 2555-15
N Top
W
W
E
E
S Base
J_n/J_{nmax} $J_{nmax} = 1.12 \times 10^{-3}$A/m
Scale division = 205×10^{-6} A/m
Sample 2555-17
J_n/J_{nmax} $J_{nmax} = 1.39 \times 10^{-3}$A/m
Scale division = 190×10^{-6} A/m
Sample 2555-23
J_n/J_{nmax} $J_{nmax} = 1.23 \times 10^{-3}$A/m
Scale division = 211×10^{-6} A/m
Sample 2555-25
J_n/J_{nmax} $J_{nmax} = 1.40 \times 10^{-3}$A/m
Scale division = 239×10^{-6} A/m
mT
1
2
Horizontal plane
Vertical plane

Fig. 5. Contd.

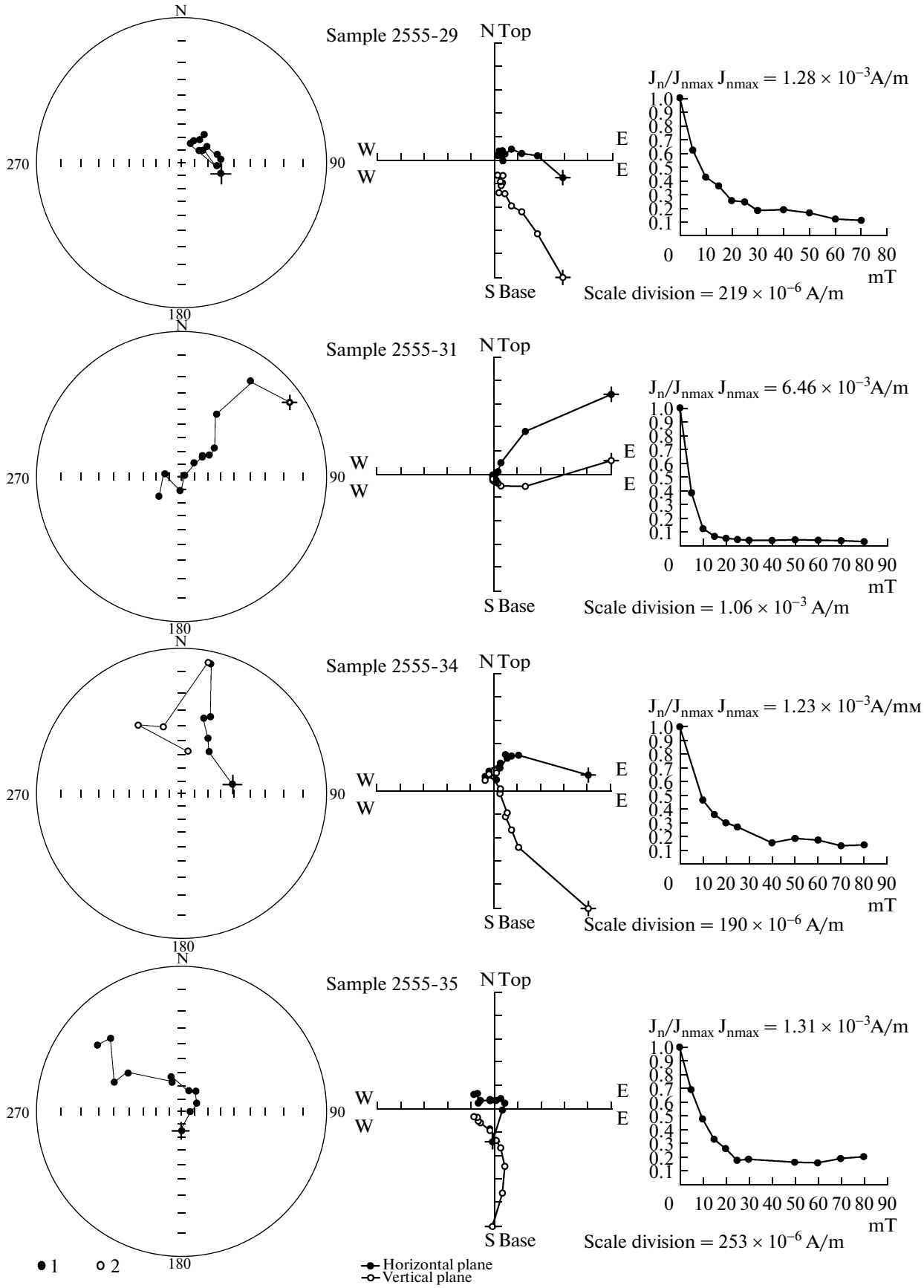
N
270
90
180
Sample 2555-29
N Top
S Base
W
E
J_n/J_{nmax} $J_{nmax} = 1.28 \times 10^{-3}$A/m
Scale division = 219×10^{-6} A/m
Sample 2555-31
J_n/J_{nmax} $J_{nmax} = 6.46 \times 10^{-3}$A/m
Scale division = 1.06×10^{-3} A/m
Sample 2555-34
J_n/J_{nmax} $J_{nmax} = 1.23 \times 10^{-3}$A/mм
Scale division = 190×10^{-6} A/m
Sample 2555-35
J_n/J_{nmax} $J_{nmax} = 1.31 \times 10^{-3}$A/m
Scale division = 253×10^{-6} A/m
0 10 20 30 40 50 60 70 80 90
mT
1
2
Horizontal plane
Vertical plane

Fig. 5. Contd.

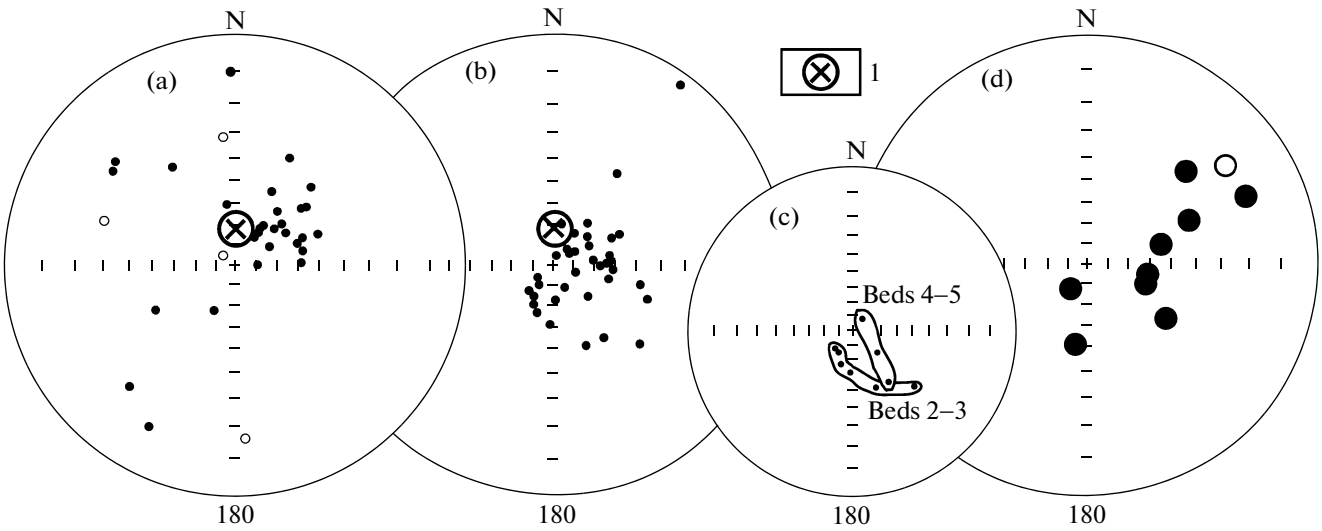

Fig. 6. Stereographic projections (a) of high-coercivity (HCC) and (b) low-coercivity (LCC) $\mathbf{J_n}$ components in the Prosek section, (c) LCC in individual beds of the section, (d) directions of the paleomagnetic field in the Middle Volga region corresponding to different positions of magnetic poles during the Goethenburg excursion.
(1) direction of the present-day geomagnetic field, for legend, see Fig. 5.

between the HCC and ChRM vector, directed toward the lower hemisphere (D = 32.9°; I = +66.8°). When (Δ) exceeded 60° of the large circle arc and the $\mathbf{J_n}$ projection regularly moved during cleanings, the high-coercivity component was considered to be controlled by the sum of the incompletely cleaned "hard" vector and primary component, corresponding to the reverse polarity of the geomagnetic field. When the angle distance was <30° and the $\mathbf{J_n}$ vector regularly migrated toward the ChRM during cleaning, the HCC direction was considered to be determined by the normal polarity of the geomagnetic field.

The paleomagnetic column constructed in such a manner (Fig. 9) demonstrates the completely regular zoning: each of the four upper magnetic zones (two with reverse (R) and two with normal (N) polarities) that comprise most of the section is substantiated by samples taken from 4–12 stratigraphic levels (Fig. 9).

Table 4. Paleomagnetic characteristics of Upper Bathonian–lower Callovian sediments in the Prosek section

Figure number	Rocks	Large circles (LC)		Intersection of LC (ChRM direction)			Apparent geomagnetic pole			φ_m°
		N	MDA°	D°	I°	MDA°	F°	L°	A_{95}°	
9a	Sands and clays	30	to 25	43.2 (223.2)	+68.2 (–68.2)	3.7	64.4	127.1	5.7	51.3
9b	Sands and clays	17	<15	38.6 (218.6)	+67.0 (–67.0)	4.4	66.1	133.9	6.6	49.7
9c	Clays	12	to 25	37.3 (217.3)	+67.0 (–67.0)	3.9	66.9	135.1	5.9	49.7
9d	Clays	9	<15	32.9 (212.9)	+66.8 (–66.8)	4.6	69.2	139.6	6.9	49.4
HCC directions in individual samples		Sample 3		36.2	+70.3	12.5				
		Sample 23		34.5	+68.3	7.6				
		Sample 25		35.8	+66.2	9.9				
Standard poles for the North Eurasian Plate (Molostovskii and Khramov, 1997)					173 Ma		65	132	10.5	
					151 Ma		69	131	9.4	
Standard poles for stable Europe (Besse and Courtillot, 2002)			Averaging window 10 Ma		150 Ma		75.0	159.9	6.6	
					160 Ma		72.5	144.0	5.0	
					170 Ma		69.7	112.5	6.7	
			Averaging window 5 Ma		155 Ma		74.3	137.4	3.5	
					160 Ma		71.9	149.7	7.1	
					165 Ma		70.6	149.5	9.7	
					170 Ma		70.1	129.9	7.7	

Note: (*N*) number of samples; (D, I) declination and inclination of the paleomagnetic vector, respectively; (MDA) maximal deviation angle; (F, L, A_{95}) latitude, longitude, and radius of the confidence circle for the apparent geomagnetic pole, respectively; (φ_m) paleomagnetic latitude. In the formulas of the A_{95} calculation, based on the ChRM direction, the MDA value for the average paleomagnetic vector (a_{95}) was used instead of the confidence circle.

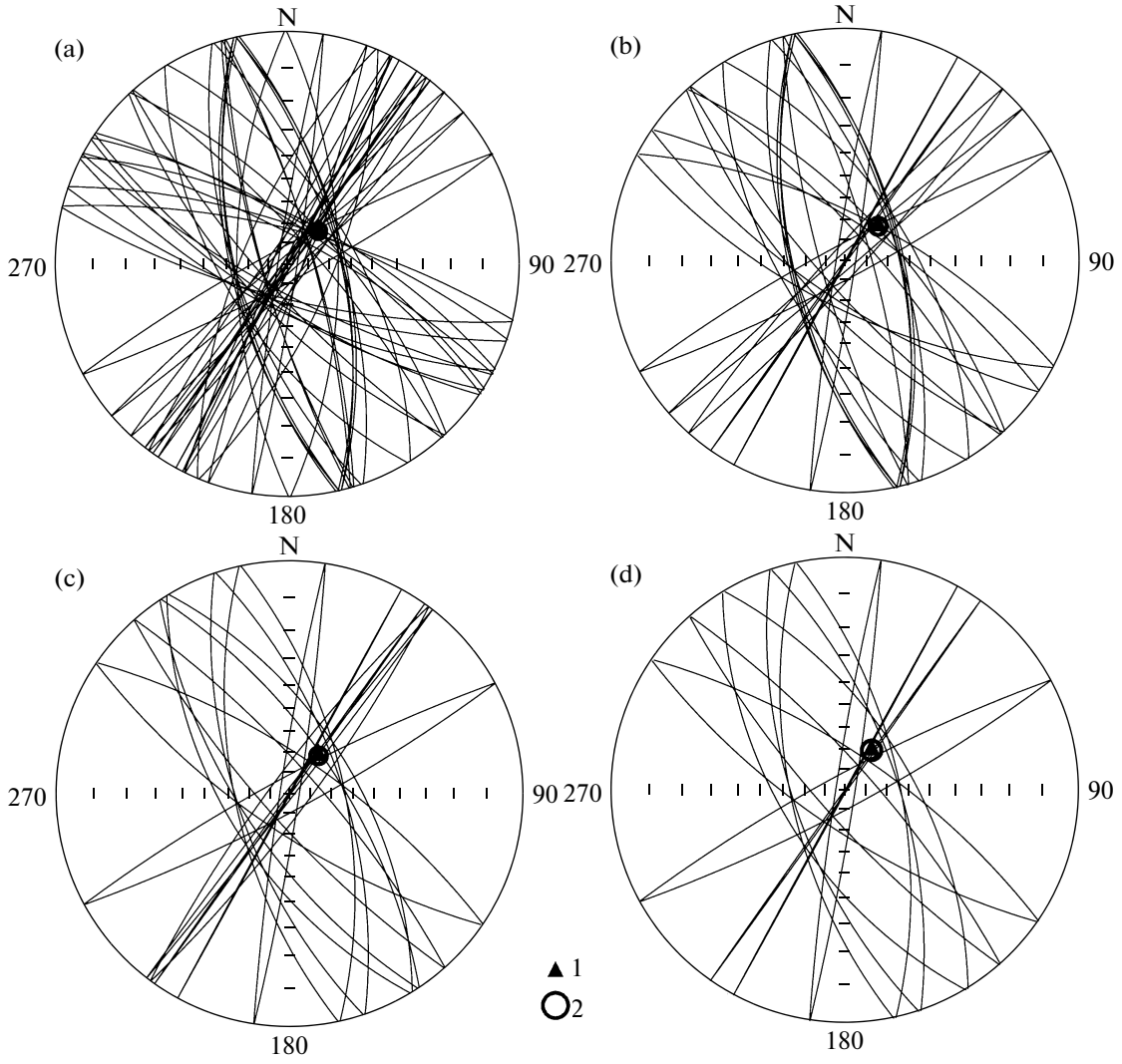

Fig. 7. Determinations of the $\mathbf{J_n}$ characteristic component (ChRM) by the method of intersection of large circles (LC). (1) ChRM direction corresponding to the point of LC intersection; (2) circle with radius equal to the maximal deviation angle (MDA); characterizes the quality of ChRM determination.

Polarities based on samples taken from one–two levels are shown as half of the column width (Fig. 9). The polarity determined for samples 1 and 2 from the base of the section is undeterminable, since they are characterized by the one-component $\mathbf{J_n}$ composition, corresponding to the remagnetization direction. The high-coercivity directions of magnetization in the three-component Sample 17 are projected on the upper hemisphere (Fig. 5), which allows its HCC to be considered as being determined by the reverse polarity. At the same time, the large circle, determined by using the $\mathbf{J_n}$ directions in fields of 25–80 mT, is located away from the ChRM directions. It can be assumed that the primary magnetization of Sample 17 was formed in the anomalous geomagnetic field, particularly taking into consideration the fact that the latter was taken at the transition between different-polarity zones. No paleomagnetic (and petromagnetic) measurements were conducted for Sample 37 due to its very strong alteration by supergene processes.

Indirect, although important, evidence in favor of the responsibility of the polar regime of the old geomagnetic field for the formation of magnetic zones is provided by the indifferential reaction of the magnetic polarity to lithology, mineral composition, and variations in petromagnetic characteristics, reflecting the properties of the magnetic fraction. Reversals of the geomagnetic field are global events; therefore, for particular sections with primary magnetization, the probability of the coincidence of paleomagnetic boundaries with interfaces, determined by local and regional factors, is insignificant. The neutral reaction of the geomagnetic polarity to the lithology of the examined sediments is evident (Figs. 2, 9) and represents,

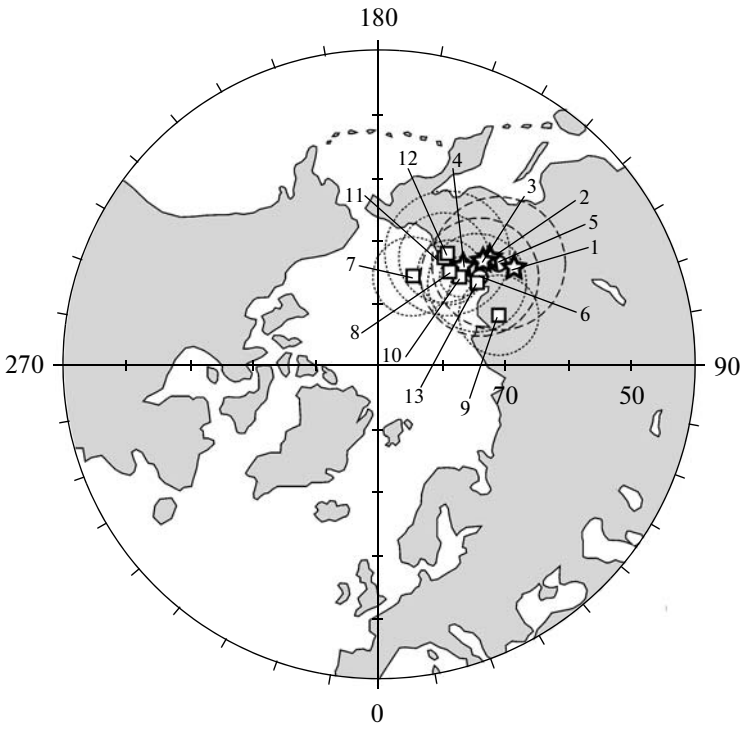

Fig. 8. Positions of virtual geomagnetic poles (VGMP) determined for Middle–Upper Jurassic sediments.
Asterisks (1–4) VGMP calculated using ChRM defined in the Prosek Section; circles (5–6) standard poles available for the North Eurasian Plate (Molostovskii and Khramov, 1997), confidence circles (A_{95}) for them are designated by dashed line; squares (7–13) standard poles for stable Europe (Besse and Courtillot, 2002), A_{95} for them are designated by the dotted line (Table 4).

together with the above-mentioned facts, such as the closeness of the calculated virtual geomagnetic poles to their standard positions (Fig. 8, Table 4) and the regular structure of the paleomagnetic column (Fig. 9), a weighty argument in favor of the geophysical nature of the defined magnetic polarity zones.

An important factor indicating the old nature of magnetization is the "criterion of external similarity", i.e., the identity of the paleomagnetic structure of coeval sediments in remote sections. The larger the lithological—facies' geostructural differences between compared sections, the more valuable is the criterion of the external similarity for substantiating the primary $\mathbf{J_n}$ nature. As a whole, the paleomagnetic zonality of the Prosek section is consistent with the traditional concepts of the complex sign-variable regime of the geomagnetic field at the Bathonian–Callovian transition, based on the linear magnetic anomalies and paleomagnetic study of deep-sea drilling cores and sections in West Europe (Ogg and Ogg, 2008).

The magnetic polarity data on the Prosek section may be compared only with similar information on the *Albstadt–Pfeffingen section* (Germany), which also demonstrates the most complete succession of the Bathonian–Callovian boundary sediments. The information on the paleomagnetic structure of the German section (Fig. 10) is based on (Callomon and Dietl, 2002), where the authors provide a generalized magnetostratigraphic characteristic (without an illustration of the paleomagnetic column) and private communication with J. Ogg (2008), who kindly permitted the use of unpublished results of his paleomagnetic analysis. Similar to the Prosek section, the Albstadt–Pfeffingen section is highly transformed by weathering processes, determining rock remagnetization, which hampers the identification of their polarity: segments of the paleomagnetic section in Fig. 10, with the polarity sign shown as a half-column allow alternative interpretations. Nevertheless, J. Ogg outlined presumably several intervals with a reverse polarity, against a background of predominantly normal polarity, including the largest zone of reverse polarity in the upper part of the *hochstetteri* and the basal part of the *keppleri* biohorizons. A comparison of the paleomagnetic columns of the Prosek and Albstadt–Pfeffingen sections shows that they are strongly consistent: in both of them, the Bathonian–Callovian boundary is characterized by the R magnetic zone, complicated by two intervals of opposite polarity; the interval of the reversed polarity within the *infimum* biohorizon can represent an analog of a similar interval within the *orbis* biohorizon. The results of the paleomagnetic correlation are completely consistent with the correlation variant of the Bathonian–Callovian infrazonal scales proposed in (Kiselev and Rogov, 2007). Thus, despite the fact that the interpretation of the magnetic polarity in each of the sections may vary, the similarity

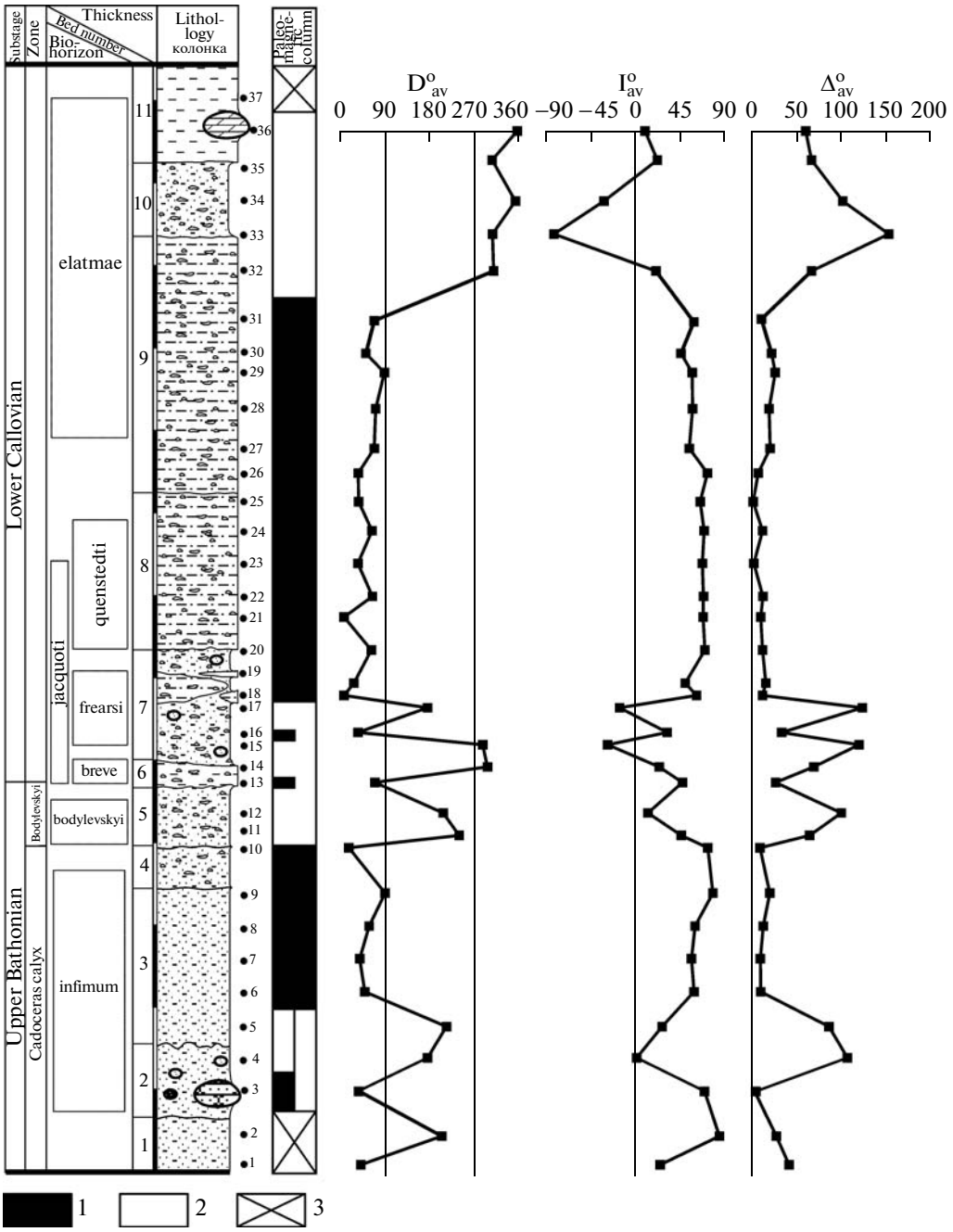

Fig. 9. Magnetostratigraphy of the upper Bathonian–lower Callovian sediments in the Prosek section (Nizhni Novgorod region). (1) normal polarity; (2) reversed polarity; (3) no data on polarity. For legend, see Fig. 2.

in the paleomagnetic structure in these two remote sections represents the best argument in favor of the correct reconstructions of the old field in the Prosek area.

A comparison of the magnetostratigraphic data on the Posek section and the Bathonian–Callovian boundary interval in northern Italy (Channell et al., 1990) and southern Spain (Steiner et al., 1987) cannot be considered as reliable. In the Italian sections, the top of the Bathonian corresponds to the major hiatus; in addition, the age of the boundary sediments is determined only at the stage level. The basal Callovian layers (*Bullatus* Zone represented by a single layer approximately 10-cm thick), substantiated only in the Covolo di Camposilvano, are marked by the replacement of the reversed polarity by the normal one. In addition, the beds attributed to the *Bullatus* Zone are most likely younger, compared with the uppermost part of the examined Prosek section. The Spanish sections include only the uppermost Bathonian sediments; moreover, the top of the stage is marked by a major hiatus.

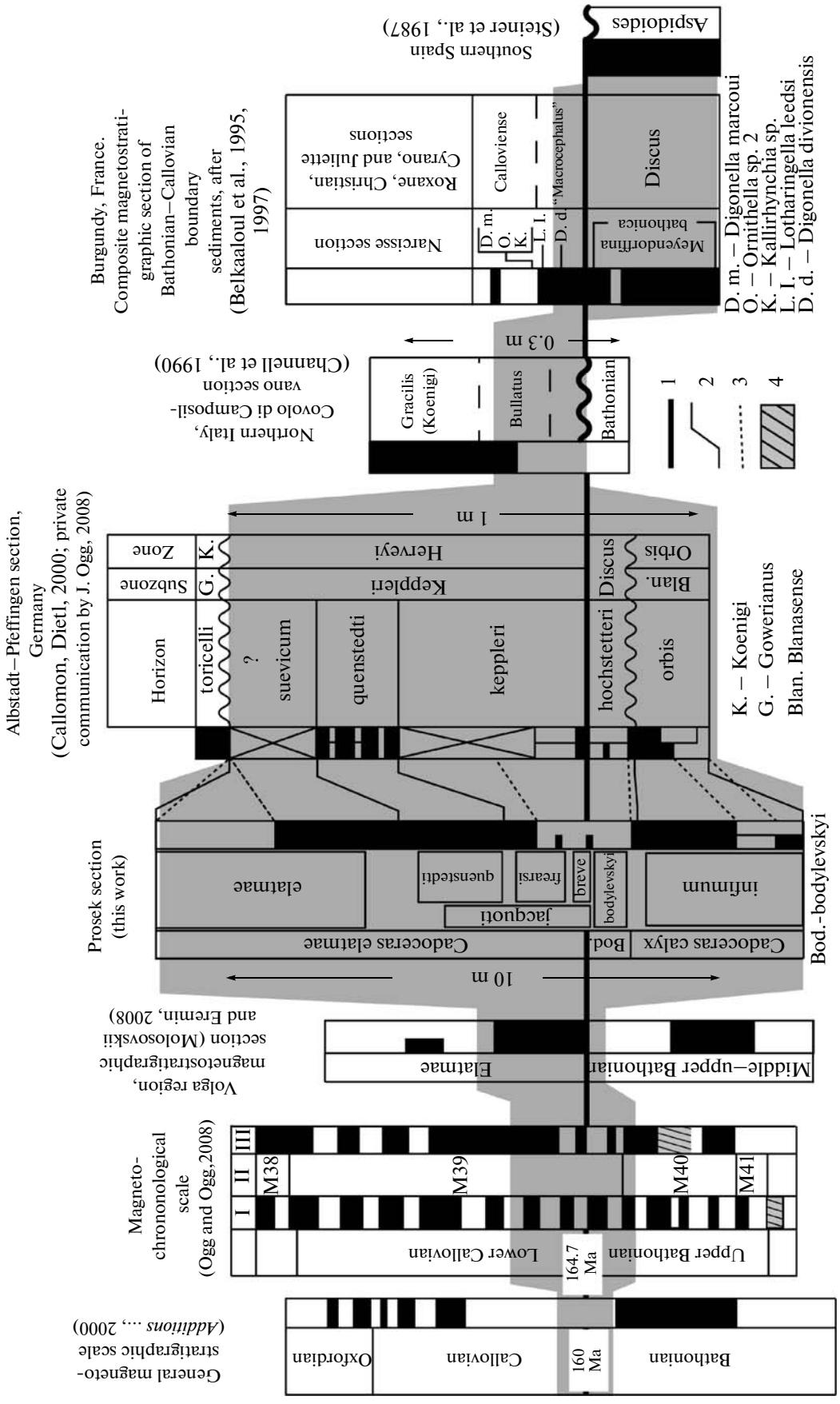
General magneto-stratigraphic scale (Additions ..., 2000)
Bathonian
Callovian
Oxfordian
160 Ma
164.7 Ma
Upper Bathonian
Lower Callovian
Magneto-chronological scale (Ogg and Ogg,2008)
I
II
III
M38
M39
M40
M41
Volga region, magnetostratigraphic section (Molosovskii and Eremin, 2008)
Middle–upper Bathonian
Elatmae
Prosek section (this work)
10 m
Cadoceras elatmae
Bod.
Cadoceras calyx
elatmae
jacquoti
quenstedti
frearsi
breve
bodylevskyi
infimum
Bod.-bodylevskyi
Albstadt–Pfeffingen section, Germany (Callomon, Dietl, 2000; private communication by J. Ogg, 2008)
1 m
Horizon
Subzone
Zone
toricelli
? suevicum
quenstedti
keppleri
hochstetteri
orbis
Discus
Blan.
Orbis
K.
G.
Herveyi
Keppleri
K. – Koenigi
G. – Gowerianus
Blan. Blanasense
Northern Italy, Covolo di Camposil-vano section (Channell et al., 1990)
Gracilis (Koenigi)
Bullatus
Bathonian
0.3 m
1
2
3
4
Burgundy, France. Composite magnetostrati-graphic section of Bathonian–Callovian boundary sediments, after (Belkaaloul et al., 1995, 1997)
Narcisse section
Roxane, Christian, Cyrano, and Juliette sections
D. m.
O.
K.
L. I.
D. d. "Macrocephalus"
Calloviense
Discus
Meyendorffina bathonica
D. m. – Digonella marcoui
O. – Ornithella sp. 2
K. – Kallirhynchia sp.
L. I. – Lotharingella leedsi
D. d. – Digonella divionensis
Southern Spain (Steiner et al., 1987)
Aspidoides

Fig. 10. Correlation of magnetostratigraphic data on Bathonian–Callovian sections from different regions.
(I) geomagnetic polarity derived from linear magnetic anomalies and analysis of deep-sea drilling cores; (II) magnetic polarity chrons; (III) polarity derived from the study of European sections (Spain, France, England, Germany). (1) Bathonian–Callovian boundary; (2) lines of infrazonal biostratigraphic correlation (Kiselev and Rogov, 2007); (3) lines of paleomagnetic correlation; (4) anomalous polarity. For other polarity symbols, see Fig. 9.

The paleomagnetic correlation between the upper Bathonian–Callovian sediments of the Volga region and Burgundy (Belkaaloul et al., 1995, 1997) (Fig. 10) reveals that the Prosek section is stratigraphically more complete as compared with the coeval sediments of France, since they lack analogues of reverse polarity magnetic zones, established at the Bathonian–Callovian transition and within the *elamatae* biohorizon of the Prosek section. The basal reverse polarity zone in the Callovian Stage of Burgundy is registered in the *Calloviense* Zone, which is unambiguously younger than beds sampled in the Nizhni Novgorod region. The magnetic zone with the reverse polarity, outlined for samples taken from two levels in the *infimum* biohorizon in the Prosek section, represents probably an analogue of the *R* zone in the upper Bathonian part of the Narcisse section.

The magnetostratigraphic Prosek section is consistent also with the paleomagnetic data on the Volga region, obtained for the Callovian Malinovyi Ravine reference section (Saratov region) and the cores of prospecting wells in the Saratov Trans-Volga region (Molostovskii and Eremin, 2008) (Fig. 10).

As for the General magnetostratigraphic scale (*Additions* ..., 2000) (Fig. 10), information on the monopolar reverse magnetic regime of the field at the Bathonian–Callovian transition should be revised.

CONCLUSIONS

(1) The Prosek section is characterized by a rhythmic structure. Based on the combined analysis of clay minerals and grain-size composition, three large sedimentary cycles, complicated by smaller cycles and the beginning of the fourth one, are definable. The first stage was marked by shallow-water settings with high-energy hydrodynamics. At the end of this stage, such a regime was replaced by transgression, which was intermittently interrupted by local regressions during the second stage. The third stage was characterized by the transgressive trend despite local sea-level fluctuations and the general tendency for its cessation at the beginning of this stage. The fourth stage was marked by the wide development of a new transgression.

(2) According to the mineral analysis of the heavy fraction's composition, petromagnetic properties, and grain-size composition, this section is also divisible into four members, corresponding to different stages in the development of the paleobasin. The boundaries between members are marked by distinct changes in the proportions of unstable and stable minerals, grain-size composition, and the distribution of petromagnetic characteristics. Changes in different lithological characteristics reflect sedimentary rhythms and are related largely to variations in the intensity of the terrigenous material transported into the paleobasin, which was controlled, in turn, by sea-level fluctuations due to eustatic or (and) tectonic factors. All the obtained data indicate the low sea-level in the terminal Bathonian and the development of the transgression since the beginning of the Callovian. The main share of terrigenous material was received from the northern land, which is evident from the similarity between the mineral spectra of heavy fractions from the Prosek section and the crystalline rocks of the Baltic Shield.

At the same time, all the boundaries between the defined members are relatively gradual, indirectly indicating the lack of any significant breaks in sedimentation, which are usually accompanied by jumpwise changes in rock lithology.

(3) The method of the intersection of large circles was used for identifying the characteristic magnetization component. The main argument in favor of its primary origin is the practically complete coincidence of the positions calculated for virtual geomagnetic poles with the coeval standard poles available for Europe. The magnetic polarity signs determined for some samples are ambiguous. At the same time, the proposed variant of the magnetostratigraphic column is strongly consistent with independent paleomagnetic data on the Albstadt–Pfeffingen section and the results of the biostratigraphic infrazonal correlation between the Bathonian–Callovian sediments of the Russian Plate and West Europe (Germany), which substantially increases the reliability of the reconstructions of the magnetic polarity. The record of the polarity regime of the paleomagnetic field in the Prosek section area is the most complete one for the Bathonian–Callovian boundary interval, which is evident from the results of the magnetostratigraphic correlation. According to its paleomagnetic information, the Prosek section is comparable to the Albstadt–Pfeffingen section; moreover, it is more preferable as compared with the latter. This fact combined with the lack of major gaps in sedimentation and the significantly higher thickness (an order of magnitude) of the basal Callovian sediments make the Prosek section a more preferable candidate for the GSSP standard of the Callovian Stage.

ACKNOWLEDGMENTS

We are grateful to P. Pruner and other colleagues from the Institute of Geology of the Czech Academy of Sciences (Prague), who performed paleomagnetic measurements on the cryogenic magnetometer, and J. Ogg from Purdue University (West Lafayette), who allowed the use of his unpublished paleomagnetic data

on the Albstadt–Pfeffingen section. We thank also M.A. Rogov (Geological Institute of the Russian Academy of Sciences) for numerous recommendations, which improved the manuscript. This work was supported by the Russian Foundation for Basic Research, project nos. 08-05-00385, 07-05-01026, 06-05-64284, and 09-05-00456.

Reviewers V.A. Zakharov,
D.N. Kiselev, and M.A. Rogov

REFERENCES

1. *Additions to the Stratigraphic Code of Russia* (VSEGEI, St. Petersburg, 2000) [in Russian].
2. K. N. Belkaaloul, D. M. Aissaoui, M. Rebelle, and G. Sambet, "Magnetostratigraphic Correlation of the Jurassic Carbonates from the Paris Basn: Implications for Petroleum Exploration," J. Geol. Soc. London **95**, 173—186 (1995).
3. K. N. Belkaaloul, D. M. Aissaoui, M. Rebelle, and G. Sambet, "Resolving Sedimentological Uncertainties Using Magnetostratigraphic Correlation: An Example from the Middle Jurassic of Burgundy, France," J. Sed. Res. **67**, 676–685 (1997).
4. J. Besse and V. Courtillot, "Apparent and True Polar Wander and the Geometry of the Geomagnetic Field over the Last 200 Myr," J. Geophys. Res. **107** (11), 1–31 (2002).
5. J. H. Collomon and G. Dietl, "On the Proposed Basal Boundary Stratotype (GSSP) of the Middle Jurassic Callovian Stage," GeoResearch Forum **6**, 41–54 (2000).
6. J. E. T. Channel, F. Massari, A. Benetti, and . Pezzoni, "Magnetostratigraphy and Biostratigraphy of Callovian–Oxfordian Limestones from the Trento Plateau (Monti Lessini. Northern Italy), "Palaeogeogr., Palaeoclimatol., Palaeoecol. **79**, 289–303 (1990).
7. V. A. Grossgeim, *Terrigenous Sedimentation in the European Part of the USSR during the Mesozoic and Cenozoic* (Nedra, Leningrad, 1972) [in Russian].
8. V. A. Grossgeim, O. V. Beskrovnaya, I. L. Gerashchenko, et al., *Methods of Paleogeographic Reconstructions (in Prospecting oil and Gas Accumulations)* (Nedra, Leningrad, 1984) [in Russian].
9. D. B. Gulyaev and D. N. Kiselev, "Boreal Upper Bathonian in the Volga River Middle Courses (Ammonites and Stratigraphy)," Stratigr. Geol. Korrelyatsiya **7** (3), 79–94 (1999) [Stratigr. Geol Correlation **7**, 279–293 (1999)].
10. H, C, Halls, "A Least-squares Method to find a Remanence Direction from Converging Remagnetization Circles," Geophys. J. R. Astr. Soc. **45**, 297–304 (1976).
11. Yu. N. Karogodin, *Stratigraphic Cyclicity* (Nedra, Moscow, 1980) [in Russian].
12. D. N. Kiselev and M. A. Rogov, "Stratigraphy of the Bathonian–Callovian Boundary Deposits in the Prosek Section (Middle Volga Region). Article 1. Ammonites and Infrazonal Biostratigraphy," Stratigr. Geol. Korrelyatsiya **15** (5), 42–73 (2007) [Stratigr. Geol Correlation **15**, 485–515 (2007)].
13. E. A. Molostovskii and V. N. Eremin, "Magnetostratigraphy of Jurassic Sediments in the Volga River Lower and Middle Courses," Byul. MOIP. Otd. Geol. **83** (4), 43–53 (2008).
14. E. A. Molostovskii and A. N. Khramov, *Magnetostratigraphy and Its Significance for Geology* (Saratov University, Saratov 1997) [in Russian].
15. J. Ogg and G. Ogg, "Late Jurassic (139–169 Ma timeslice," (2008)//URL:http://www.nhm.uio.no/norges/timescale/5_JurCret_Sept08.pdf
16. G. A. Pospelova, "Geomagnetic Excursions during the Brunhes Chron and Global Climatic Oscillations," Physics of the Earth, No. 8, 3–14 (2000).
17. D. Sahagian, O. Pinous, A. Olfer'ev, and V. Zakharov, "Eustatic Curve for the Middle Jurassic–Cretaceous Based on Russian Platform and Siberian Stratigraphy: Zonal Resolution," AAPG Bull. **80**, 1433–1458 (1996).
18. J. Sandoval, L. Doherty, and J. Guex, "Evolutionary Rates of Jurassic Ammonites in Relation to Sea-level Fluctuations," PALAIOS **16**, 311–335 (2001).
19. I. G. Sazonova and N. T. Sazonov, *Paleogeography of the Russian Platform in the Jurassic–Early Cretaceous* (Nedra, Leningrad, 1967) [in Russian].
20. A. Seilacher, *Trace Fossil Analysis* (Springer, New York, 2007).
21. M. V. Steiner, J. G. Ogg, and I. Sandoval, "Jurassic Magnetostratigraphy, Bathonian–Bajocian of Carcabucy, Sierra Harana and Campillo de Arenas (Subbetic Cordillera, Southern Spain)," Earth Planet. Sci. Lett. **82**, 357–372 (1987).
22. A. N. Tretyak, *Natural Remanent Magnetization and Problem of Paleomagnetic Stratification of sedimentary Sequences* (Naukova Dumka, Kiev, 1983) [in Russian].